SOUTHERN PLAINS
TRANSPORTATION CENTER

Risk-Based Life-Cycle Management of Deteriorating Bridges

Mohamed Soliman, Ph.D.
Omid Khandel,
Julie A. Hartell, Ph.D.

SPTC15.1-12-F

TECHNICAL REPORT DOCUMENTATION PAGE

1. REPORT NO. SPTC15.1-12-F	2. GOVERNMENT ACCESSION NO.	3. RECIPIENTS CATALOG NO.
4. TITLE AND SUBTITLE Risk-based Life-Cycle Management of Deteriorating Bridges		5. REPORT DATE March 3, 2019
		6. PERFORMING ORGANIZATION CODE
7. AUTHOR(S) Mohamed Soliman, Omid Khandel, and Julie A. Hartell		8. PERFORMING ORGANIZATION REPORT
9. PERFORMING ORGANIZATION NAME AND ADDRESS School of Civil & Environmental Engineering Oklahoma State University 207 Engineering South Stillwater, Oklahoma 74078		10. WORK UNIT NO.
		11. CONTRACT OR GRANT NO. DTRT13-G-UTC36
12. SPONSORING AGENCY NAME AND ADDRESS Southern Plains Transportation Center 201 Stephenson Pkwy, Suite 4200 The University of Oklahoma Norman, OK 73019		13. TYPE OF REPORT AND PERIOD COVERED Final March 2016 – September 2018
		14. SPONSORING AGENCY CODE
15. SUPPLEMENTARY NOTES University Transportation Center		

16. ABSTRACT

Bridges are subjected to continuous deterioration due to aging, mechanical stressors, and harsh environmental conditions. Among these threats, hydraulic-related ones are identified as the leading cause of bridge failure in United States. Failure or closure of the bridges can cause a significant drop in transportation system functionality and consequently leads to severe economic and social impacts. A proper maintenance and repair strategy for extending the service life of deteriorating bridges can be achieved through comprehensive risk-based approaches. Since flood frequency is expected to change as a result of global climate change, proper prediction of future flood hazard becomes an essential task. In addition, flood occurrence generally increases the rate of riverbed erosion, which causes the formation of scour and increases the risk of bridge failure. The scour formation highly depends on the type of bridge foundation and the river characteristics. This report presents an integrated probabilistic framework for quantifying the risk of bridge failure due to flood events considering climate change. An analytical model is integrated into a probabilistic simulation process to quantify the time-variant performance of bridge foundations under flood and flood induced scour. The effect of adopted global climate scenarios on the failure risk under flood exposure is also investigated.

17. KEY WORDS Climate Change, Global Climate Models (GCM), Risk, Flood, Scour		18. DISTRIBUTION STATEMENT No restrictions. This publication is available at www.sptc.org and from the NTIS.	
19. SECURITY CLASSIF. (OF THIS REPORT) Unclassified	20. SECURITY CLASSIF. (OF THIS PAGE) Unclassified	21. NO. OF PAGES 47	22. PRICE

SI* (MODERN METRIC) CONVERSION FACTORS

APPROXIMATE CONVERSIONS TO SI UNITS

Symbol	When You Know	Multiply By	To Find	Symbol
LENGTH				
in	inches	25.4	millimeters	mm
ft	feet	0.305	meters	m
yd	yards	0.914	meters	m
mi	miles	1.61	kilometers	km
AREA				
in^2	square inches	645.2	square millimeters	mm^2
ft^2	square feet	0.093	square meters	m^2
yd^2	square yard	0.836	square meters	m^2
ac	acres	0.405	hectares	ha
mi^2	square miles	2.59	square kilometers	km^2
VOLUME				
fl oz	fluid ounces	29.57	milliliters	mL
gal	gallons	3.785	liters	L
ft^3	cubic feet	0.028	cubic meters	m^3
yd^3	cubic yards	0.765	cubic meters	m^3
NOTE: volumes greater than 1000 L shall be shown in m^3				
MASS				
oz	ounces	28.35	grams	g
lb	pounds	0.454	kilograms	kg
T	short tons (2000 lb)	0.907	megagrams (or "metric ton")	Mg (or "t")
TEMPERATURE (exact degrees)				
^oF	Fahrenheit	5 (F-32)/9 or (F-32)/1.8	Celsius	^oC
ILLUMINATION				
fc	foot-candles	10.76	lux	lx
fl	foot-Lamberts	3.426	candela/m^2	cd/m^2
FORCE and PRESSURE or STRESS				
lbf	poundforce	4.45	newtons	N
lbf/in^2	poundforce per square inch	6.89	kilopascals	kPa

APPROXIMATE CONVERSIONS FROM SI UNITS

Symbol	When You Know	Multiply By	To Find	Symbol
LENGTH				
mm	millimeters	0.039	inches	in
m	meters	3.28	feet	ft
m	meters	1.09	yards	yd
km	kilometers	0.621	miles	mi
AREA				
mm^2	square millimeters	0.0016	square inches	in^2
m^2	square meters	10.764	square feet	ft^2
m^2	square meters	1.195	square yards	yd^2
ha	hectares	2.47	acres	ac
km^2	square kilometers	0.386	square miles	mi^2
VOLUME				
mL	milliliters	0.034	fluid ounces	fl oz
L	liters	0.264	gallons	gal
m^3	cubic meters	35.314	cubic feet	ft^3
m^3	cubic meters	1.307	cubic yards	yd^3
MASS				
g	grams	0.035	ounces	oz
kg	kilograms	2.202	pounds	lb
Mg (or "t")	megagrams (or "metric ton")	1.103	short tons (2000 lb)	T
TEMPERATURE (exact degrees)				
^oC	Celsius	1.8C+32	Fahrenheit	^oF
ILLUMINATION				
lx	lux	0.0929	foot-candles	fc
cd/m^2	candela/m^2	0.2919	foot-Lamberts	fl
FORCE and PRESSURE or STRESS				
N	newtons	0.225	poundforce	lbf
kPa	kilopascals	0.145	poundforce per square inch	lbf/in^2

*SI is the symbol for the International System of Units.   Appropriate rounding should be made to comply with Section 4 of ASTM E380. (Revised March 2003)

iii

RISK-BASED LIFE-CYCLE MANAGEMENT OF DETERIORATING BRIDGES

Final Report

March 3, 2019

Mohamed Soliman, Ph.D.

Assistant Professor

Omid Khandel, Doctoral Student

Graduate Research Assistant

and

Julie A. Hartell, Ph.D.

Assistant Professor

School of Civil & Environmental Engineering

Oklahoma State University

Stillwater, OK 74078

TABLE OF CONTENTS

LIST OF FIGURES

LIST OF TABLES

EXECUTIVE SUMMARY

Performance of transportation systems is directly linked to the economic development of societies on local, national, and global scales. An efficient transportation system should support the economic growth by reducing the travel time of passengers and goods, decreasing transportation cost, and maintaining connectivity between different markets and critical origin/destination points. Bridges are recognized as key components in ground transportation systems. These structures are vulnerable to several deterioration mechanisms which may cause gradual deterioration or sudden failures. These mechanisms can cause a significant drop in the transportation system functionality leading to severe economic and social impacts. Natural hazards (e.g., floods and earthquakes), environmental stressors (e.g., corrosion), and man-made extreme events (e.g., blast explosions and fires) are recognized as the main sources that drive bridge deterioration. Since some of these hazards (e.g., corrosion and floods) may be related to long-term climate behavior, climate change can significantly affect the performance of bridges under these hazards.

Deteriorating bridges require maintenance and repair activities to extend their service life and maintain a satisfactory performance level. These maintenance actions can lead to indirect costs associated with traffic delays and environmental impacts, in addition to the direct cost of maintenance actions, which can significantly increase the life-cycle cost of the bridge under consideration. Accordingly, these indirect effects should be considered for the proper life-cycle management of deteriorating bridges. Quantifying the uncertainties associated with different hazards and deterioration mechanisms should be included in maintenance planning while considering effects of climate change. Furthermore, an optimized maintenance planning to minimize the direct (e.g., structural rehabilitation costs) and indirect costs (e.g., traffic delays and environmental effects) should be performed with climate change in mind.

This report presents a probabilistic framework for risk assessment of bridges under flood and flood induced scour considering climate change. The flood and streamflow prediction is performed using Global Climate Models. The downscaled precipitation and temperature climate data are adopted from the Coupled Model Inter-comparison Project

Phase 5 (CMIP5) archive for the location of interest during the time span of 1960 to 2100. Time-dependent scour depth is quantified and its effect on the axial and lateral capacity of the bridge foundation is evaluated. The annual point-in-time failure probability of the bridge due to flood-induced loads is used to predict the cumulative failure probability profiles of the bridge. After evaluating the consequences associated with bridge failure, the time variant bridge risk profile is established. This report also discusses probabilistic approaches capable of optimizing maintenance activities of deteriorating bridges while considering climate change, direct maintenance costs, and indirect impact arising from maintenance and repair actions. Uncertainties associated with the various stages of the life-cycle management are discussed.

INTRODUCTION

Bridges are vulnerable to continuous deterioration due to various mechanical and environmental stressors. Among the various extreme events (e.g., earthquake, floods, and corrosive environments) which may threat the safety of bridges, hydraulic-related ones have been identified as the leading cause of bridge failure (AASHTO 2010; Briaud et al. 2013). In the United States, more than 50% of bridges failures are attributed to hydraulic stressors such as flood and scour (Cook et al. 2015). These type of failures are highly dependent on precipitation patterns and flood events at the bridge location. In this context, the National Oceanic and Atmospheric Administration (NOAA) reported an average increase of 612% in the number of floods in the United States since the 1960s; future increase in this percentage is also possible and expected (NOAA 2015). This increase in flood frequency and intensity, which may be attributed to climate change, can unfavorably affect the safety of our Nation's bridges. Subsequently, our transportation systems and the communities which they serve may experience overwhelming consequences due to the impact of climate change. As an indication on the severity of this problem, the 2015 flooding in Texas and Oklahoma led to at least five reported complete or partial bridge failures, 31 deaths, and more than $2.5 billion in economic losses to the region (Fechter 2015; Danner and Fuller 2015; Smith et al. 2017). As a result, bridge design and management approaches should consider climate change in quantifying the future flood hazard.

Prediction of future temperature, precipitation, regional moisture, rainfall, and river streamflow can be subjected to significant uncertainty due to climate change. Traditional design methods relying on return periods (i.e., 50, 100, or 500 year floods) may not provide reliable results. Accordingly, in order to improve future predictions, more advanced computational tools such as global climate modeling should be adopted. Global Climate Models (GCMs) provide a numerical representation of chemical, physical, and biological aspects of global climate system. Downscaling methods should next be used for deriving regional climate information from the adopted global scale data. For the proper implementation of these models, different types of GCMs, scenarios of future greenhouse gas (GHG) emission, and downscaling methods should be considered.

The Couple Model Inter-comparison Project Phase 5 (CMIP5) GCMs with more than 50 different models are able to project the past and future climate data (Taylor et al. 2012). Different types of climate scenarios vary based on their atmospheric horizontal resolution and their model types. These models also take the interaction of the various natural effects such as oceans, vegetation, and land surfaces into account. (Solomon et al. 2007; Sheffield et al. 2013a,b; and Maloney et al. 2014). Since the GCM models significantly differ in their prediction of temperature, precipitation and other future climatic data, appropriate models should be selected by comparing their results to observed measurements at a given location. Along with GCM models, uncertainties in future greenhouse gases (GHG) emission are presented in term of Representative Concentration Pathways (RCPs). Different RCP values represent the change in radiative forcing of GHG from pre-industrial times to 21st century. Radiative forcing can be described as change in the balance of radiation in W/m^2 between incoming solar radiation and outgoing infrared radiation. RCP 2.6 (2.6 W/m^2), RCP 4.5 (4.5 W/m^2), RCP 6 (6 W/m^2), and RCP 8.5 (8.5 W/m^2) are 4 common RCP values. The higher RCP values represent higher predicted radiation in the future.

In order to study climate patterns associated with a given location, the global GCM data should be converted to regional scale data. This can be achieved through various methods such as running a higher resolution GCM, using boundary conditions of surrounding global climate model, and using statistical downscaling methods. Although applying the statistical methods is less complicated than the others, it can still produce highly accurate results (Laprise 2008; Coiffier 2011). Since there are several GHG emission scenarios, different global climate modeling techniques, and downscaling methods, climate researchers recommend using several scenarios. Each of these scenarios can be characterized by its own future GHG emission level, global climate model, and downscaling technique (Xue et al. 2014). Next, hydrological models, such as the variable infiltration capacity (VIC) (Liang et al. 1994) and Riverware (Zagona et al. 2001), or statistical methods (Croke et al. 2005) should be used to estimate the time-dependent river discharge and quantify the future flood hazard. Such approach has been implemented in McPherson (2016) to quantify the impact of climate change on the Red River basin.

Among various hydraulic-related sources of bridge failure, preventing and managing scour problems represent a significant challenge for bridge managers (Ettouney and Alampalli 2011). This is because scour may occur in most soils and can lead to the failure of bridge foundations and consequently the entire structure. In addition, detecting and managing the scour may represent additional challenges since its effects may not be visible. Due to the importance of this issue, researchers have focused on evaluating the effect of scour on the performance of bridges using deterministic (e.g., Govindasamy et al. 2008; Arneson et al. 2012) and probabilistic (e.g., Briaud et al. 2007; Bolduc et al. 2008) approaches. In addition, multi-hazard analysis of bridges considering scour effects has been also presented in recent years (e.g., Decò and Frangopol 2011; Wang et al. 2014; Gehl and D'Ayala 2016). However, none of these studies examined the potential influence of climate change on flood hazard and scour predictions.

This report presents a probabilistic framework for assessment of time-variant risk of bridge failure due to floods and flood-induced scour considering the future change in climate conditions. The approach uses downscaled GCM data to obtain future climate trends (e.g., precipitation and temperature profiles) under different climate scenarios. The results of streamflow predictions based on various future climate scenarios are employed to quantify the future flood hazards. The failure probability of the bridge due to flood and flood-induced scour is quantified using Monte Carlo simulation. Risk is computed by combining consequences of bridge failure including direct rebuilding cost and indirect losses arising from traffic delays due to road closure. The proposed approach is applied to the I-35 Red River Bridge located on the Texas-Oklahoma border. Additionally, an approach for risk-based management of bridges is presented.

ANALYSIS OF HISTORIC PRECIPITATION TRENDS

Climate change and global warming have been popular research topics among researchers and politicians. Regardless of personal and political opinions on global warming and climate change, most will agree that local, regional and even national climates have seen significant change over the past few decades. For instance, there has been a noticeable change in the amount and frequency at which precipitation events occur in central Oklahoma. Based on the National Climate Assessment II (Melillo et al.

2014), a temperature increase of $1.5°$ Fahrenheit since 1960 has been observed throughout the Great Plains. In addition, more unpredictable precipitation patterns, including long droughts and severe floods, have been reported. Analysis of past climate records indicated that Oklahoma was characterized with strong spring storms, hot and dry summers with relatively few showers and storms, and cold winters with few snowfall events exceeding 2-4 inches of snowfall per event. Contrasting that with observations in the recent years with frequent summer showers, less frequent spring storms, and winters seeing very little to no snowfall. These observations, although rudimentary, are an important part of the scientific process for determining changes in our local climates and inferring trends and future responses to changes. Observations alone are not sufficient to provide enough evidence for a profound understanding of what is occurring in our climate and the ramifications of subtle variations and other environmental factors.

In this report, National Aeronautic and Space Administration (NASA 2017) and National Oceanic and Atmospheric Administration's (NOAA 2017) data sets are used to support and verify observations made and provide data for historical climate analysis. Data obtained include atmospheric CO_2, precipitation records, and river discharge for the Red River along the southern border of Oklahoma. This data is plotted and trend lines are fitted so that reasonable inference can be made with very little data manipulation. From simple analysis of the various datasets, a trend between the rising CO_2 and an increase in amount and variability of rainfall affecting the drainage basin can be seen. Figure 1 shows data obtained from NASA on global atmospheric CO_2. Extrapolating this data, predicts that in the next 50 years levels of atmospheric CO_2 will exceed 500 ppm.

The effects of the rising CO_2 may be observed in precipitation data. Data obtained from NOAA tracks monthly average precipitation and calculates the deviation from monthly normal for the specific station where precipitation is measured. The deviations in monthly precipitation were plotted for 1974 to 2016 as seen in Figures 2 to 10. In these figures, "normal" baselines are produced using the observed average monthly data of 30 years. The horizontal gridline at 0 indicates no deviation from normal precipitation. The figures show that since 1974, deviations in precipitation have become increasingly variable and peaks are higher than historically recorded for several key months. The months of April, May, June, and July, which historically have been classified as dry

4

months, have seen the most drastic changes in recent years. Plotted trend lines show that these months are experiencing increasing deviations from normal precipitations levels. During the same period, the months of August, October and November are trending downward, which means that this investigated weather station is experiencing several months of increasing rainfall followed by several months of decreasing rainfall. This increase in the peak flow is directly related to flood occurrence in these areas and can potentially cause an increase in erodibility of the soil and an adverse effect on the stability of many bridges in the associated drainage basin.
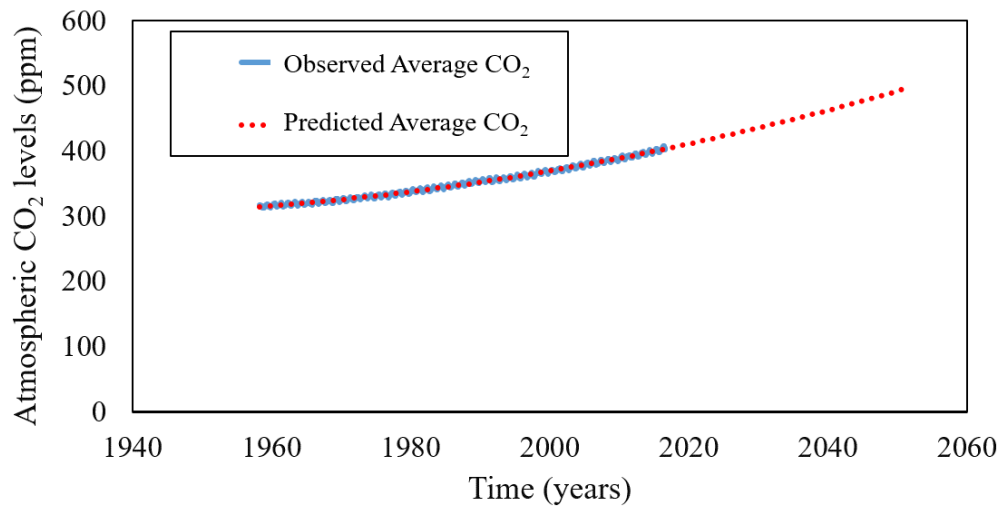

Figure 1. Average atmospheric CO_2 since 1958 (NASA 2017)
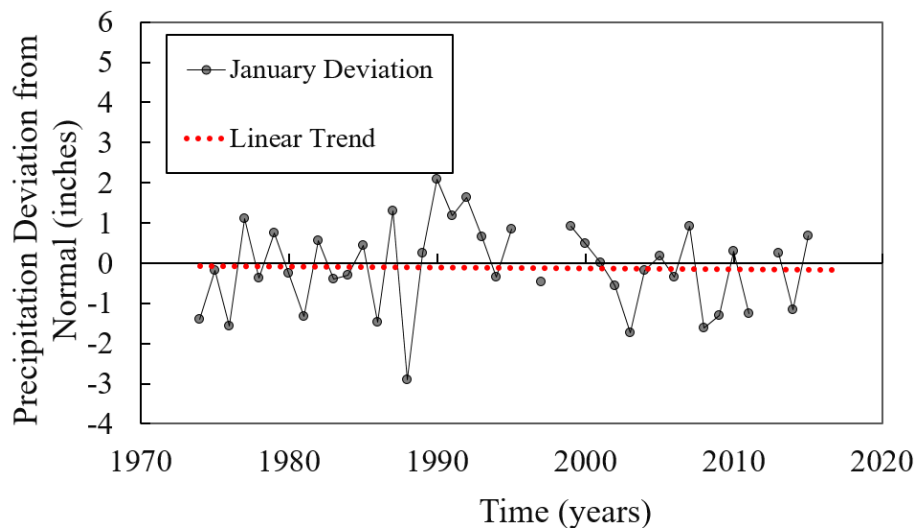

Figure 2. Precipitation deviation from normal in January since 1974

Figure 3. Precipitation deviation from normal in April since 1974.

Figure 4. Precipitation deviation from normal in May since 1974

Figure 5. Precipitation deviation from normal in June since 1974

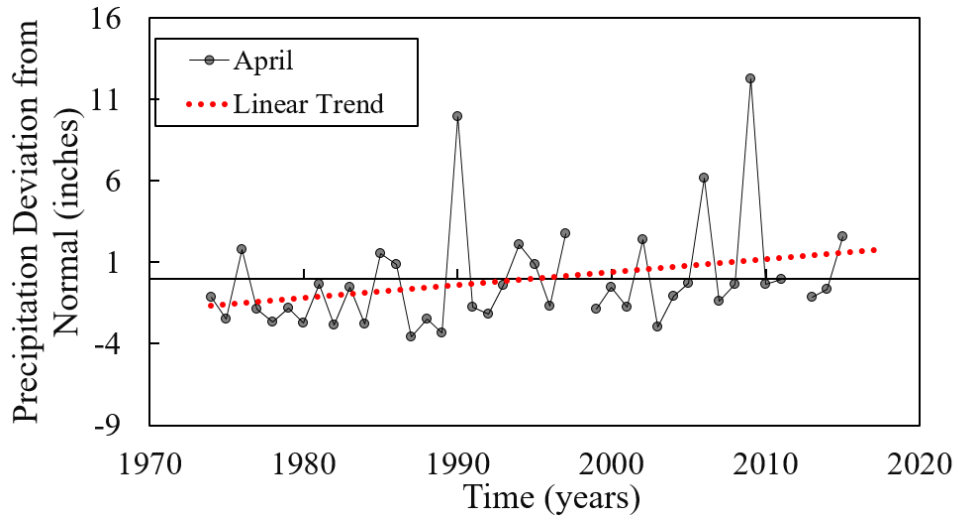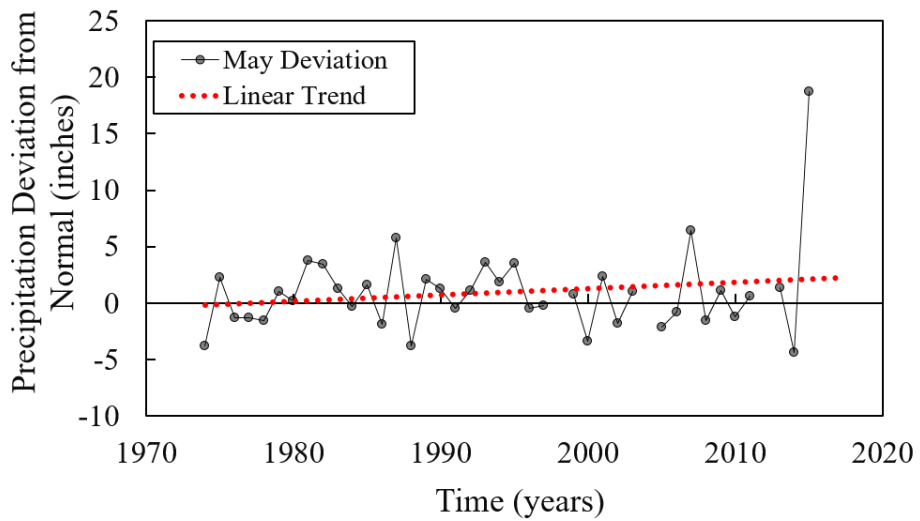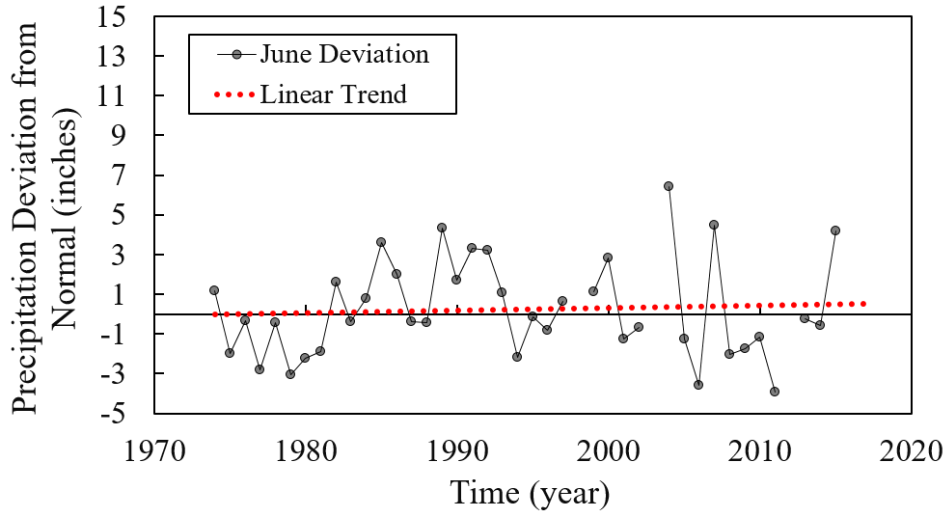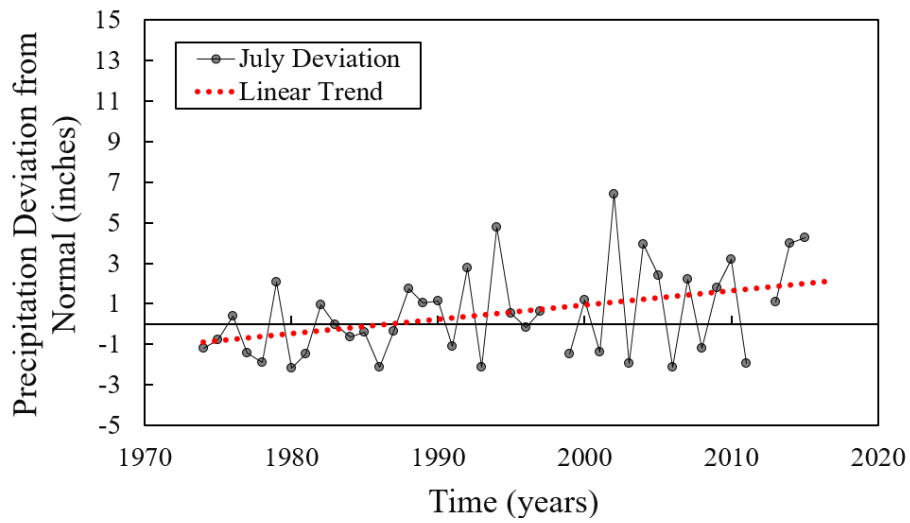**Figure 6.** Precipitation deviation from normal in July since 1974
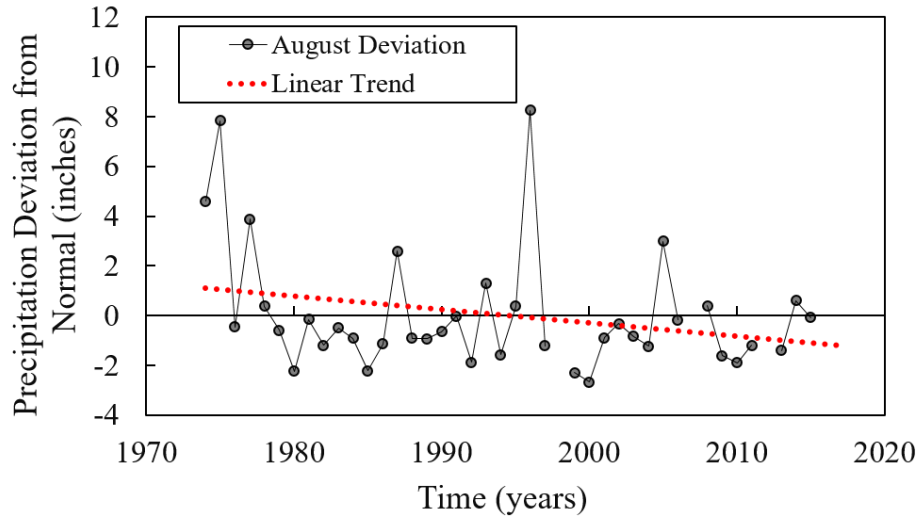
Figure 7. Precipitation deviation from normal in August since 1974
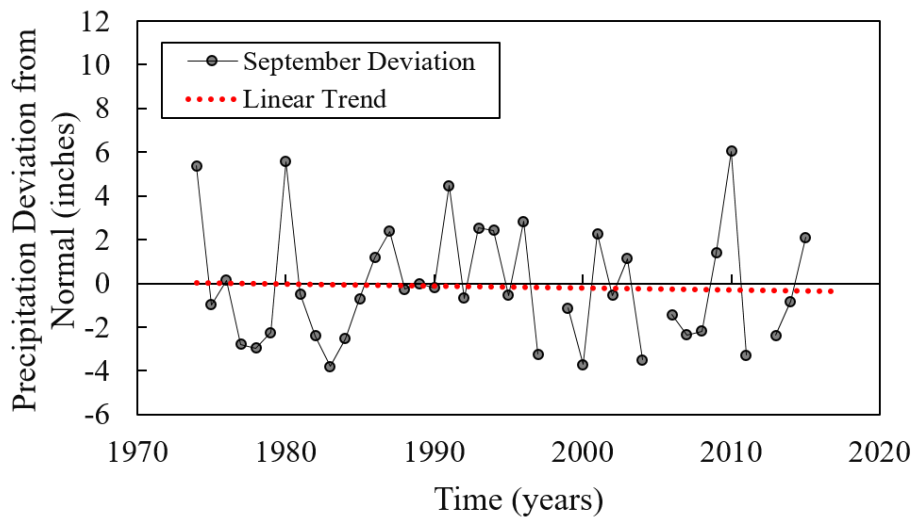
Figure 8. Precipitation deviation from normal in September since 1974
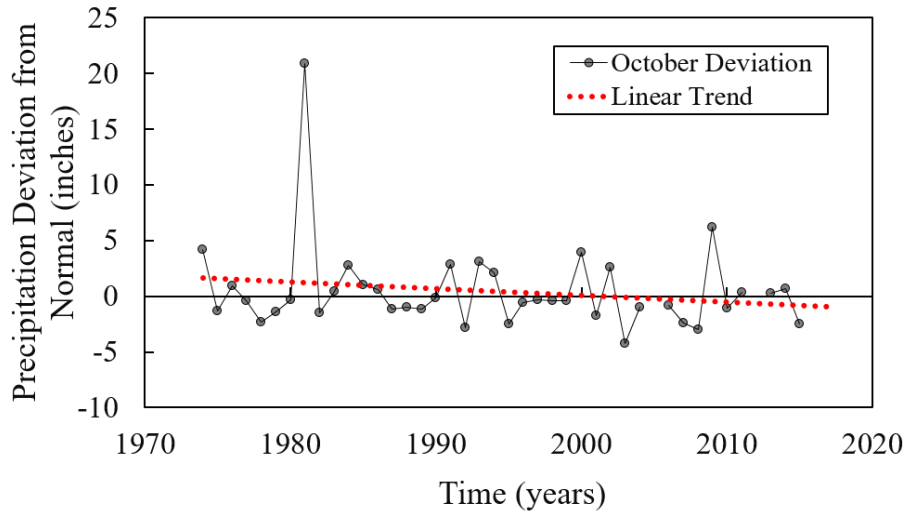
Figure 9. Precipitation deviation from normal in October since 1974
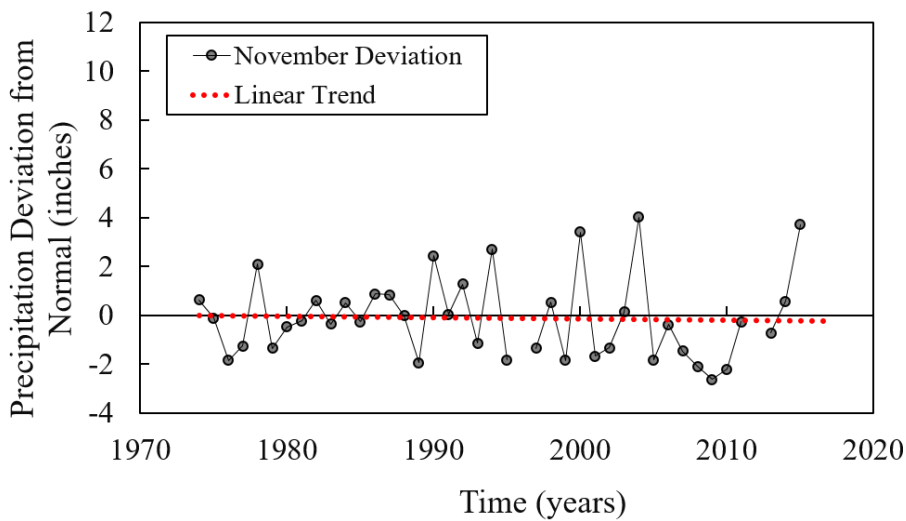
Figure 10. Precipitation deviation from normal in November since 1974

Historical data, although helpful, is limited on its ability to project into the future and provide adequate information to draw definitive conclusions on future climate trends. The use of proper climate modeling enables obtaining more accurate solutions and predictions. From these models, different scenarios can be formed by changing one or several of the model parameters. A more detailed explanation of these variables and such climate modeling is presented in the following sections of this report.

9

FUTURE CLIMATE PREDICTIONS

Climate conditions, including temperature patterns and precipitation patterns has seen considerable change in recent decades (Solomon 2007). Significant research has been directed to provide more precise future climate predictions in North and Central America (e.g., Sheffield et al. 2013a,b; Maloney et al. 2014). In particular, the Coupled Model Inter-comparison Project Phase 5 (CMIP5) is one of the widely used global climate models (GCMs) that can provide future climate projections on the near and long-term time scales (Taylor et al. 2012). This dataset includes more than 50 models that are capable of providing past and future climate data. Different types of climate scenarios differ based on their atmospheric horizontal resolution and their model types. These models also consider the interaction of various natural effects such as vegetation, oceans, and land surfaces. (Solomon et al. 2007; Sheffield et al. 2013a,b). Since the GCMs significantly differ in their prediction of temperature, precipitation and other future climatic data, they should be selected based on a comparison of their results with the available observed data at a given location.

Along with GCM models, uncertainties in future greenhouse gases (GHG) and those arising from the downscaling procedure should be considered. Different GHG emission scenarios are presented in term of Representative Concentration Pathways (RCPs). Different RCP values represent the change in radiative forcing of GHG from pre-industrial times to the 21st century. Radiative forcing can be described as change in the balance of radiation in W/m^2 between incoming solar radiation and outgoing infrared radiation. RCP 2.6 (2.6 W/m^2), RCP 4.5 (4.5 W/m^2), RCP 6 (6 W/m^2), and RCP 8.5 (8.5 W/m^2) are common RCP values. The higher RCP values represent higher predicted radiation in the future. In addition, downscaling can be performed using any acceptable downscaling method such as Bias Correction and Spatial Downscaling (BCSD), Constructed Analogues (CA), and Daily Bias Correction Constructed Analogs (BCCA). More information on these models can be found in Maurer et al. (2008 and 2010).

In order to consider all relevant future climate scenarios, different GCMs, RCP values and downscaling techniques should be examined. Such analysis has been performed by the South Central Climate Science Center (SCCSC) for the Red-River basin

(McPherson 2016) as part of a previous research project. CCSM4, MIROC5, and MPI-ESM-LR models (Gent et al. 2011; Watanabe et al. 2010; Giorgetta et al. 2013) from CMIP5 project along with three RCP values (2.6, 4.5, and 8.5) and three statistical downscaling methods has been investigated in their analysis. Cumulative Density Function transform (CDFt) (Vrac and Michelangeli 2009), Equi-distant Quantile Mapping (EDQM) (Li et al. 2010), and Bias Correction Quantile Mapping (BCQM) (Ho et al. 2012) are the three downscaling methods that adopted in their analysis.

Each RCP provides results based on a given greenhouse gas concentration. RCP2.6 uses a greenhouse model described as a peak and decline model. This accounts for the ultimate peak in greenhouse emissions and then a decline in the atmospheric concentrations of these gasses in time. RCP4.5 models make predictions based on a stabilization of the greenhouse gases around the year 2100 with no appreciable change in concentrations afterward. RCP8.5 modeling assumes that greenhouse gases continue to increase with time and no indicated stabilization. These three RCP models result in a range of possible outcomes for the global climate that span from a best case scenario to the worst case scenario. This range provides a reasonable assumption to establish boundaries for expected future climate.

The CDFt downscaling method uses a large scale Cumulative Density Function (CDF) model and calculates a mathematical transform function to apply to the data such that the resulting model is equivalent to the large-scale CDF, but focused on the smaller, local scale (Vrac and Michelangeli 2012). Equidistant quantile mapping downscaling technique is derived by taking the difference between the CDF of the global climate model and the CDF of a reference set of data. This reference set of data could be a CDF of historical observations or analysis outputs of the past climate. This difference is then subtracted from the CDF of the future climate given by the global climate model. This results in the bias correction for future global climate model data outputs (Sachindra et al. 2014).

Streamflow data was obtained from these models allowing for a comparison between RCP values of 2.6, 4.5, and 8.5. From this comparison, a reasonable determination can be made on the future expected stream flow (up to the year 2100).

These models show how differing concentrations of greenhouse gases can affect the discharge of a major river by affecting the surface temperature and precipitation for the given area. The streamflow data given by the models starts on January 1, 1961 and provides daily values until December 31, 2099. With the sheer amount of data given from these models, the data was analyzed in 12 sections with each being a month long. Two months will be illustrated in this report, the months of July and January. These two months are chosen based on the initial observation and analysis of the historical data for those months as shown in Figures 2 and 6. Figure 2 shows that in January, deviation from normal rainfall is decreasing suggesting a trend of decreasing rainfall. Figure 6 shows that the deviation from normal precipitation is increasing, meaning that from 1974 to 2015 a trend of increasing rainfall is occurring. Figures 11 and 12 show the historical discharge adopted from U.S. Geological Survey (USGS 2017) for the Red River near Gainesville, Texas for the month of January and July respectively. As shown in these figures, there is a distinct correlation between decreasing rainfall and decreasing river discharge in January, and increasing rainfall and increasing discharge in July. This correlation exists for all months and is expected.
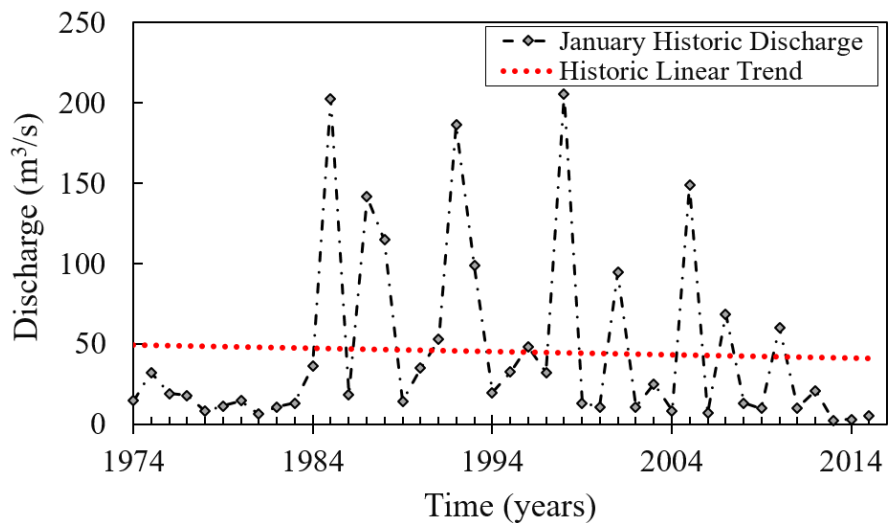

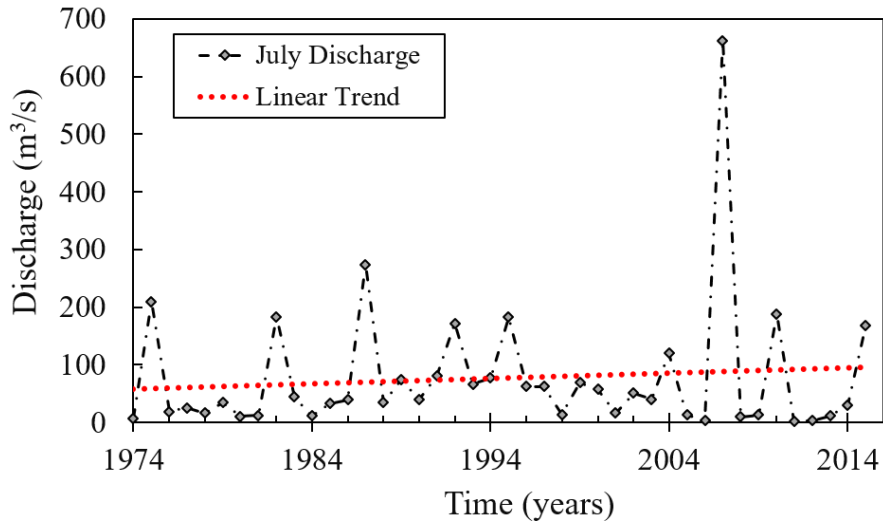**Figure 11.** Historical January discharge for the Red River 1974-2015

Figure 12. Historic July discharge for the Red River 1974-2015

Figure 13 illustrates the July river discharge resulting from one climate model adopted from McPherson (2016) and the historical data. It can be seen that the results of the model do not match historic data. This may be observed when looking at an individual climate scenario, characterized by its own GCM, downscaling technique, and RCP value, versus the historical data. Accordingly, a common practice is to use all available datasets to consider uncertainties in future streamflow prediction (Seager et al. 2007; Pierce et al. 2009). This however provides a wide range of possible bounds within the time span covered by the prediction models.

Since no reliable prediction can be made using a single climate scenario, all the climate model data was averaged every day for the months of January and July between 1974 to 2015. This was then plotted against the historical data to observe any similarity in trends on a month by month basis. It should be noted that the BCQM downscaled data was not included due to inaccuracies stated in Wayne (2013). Figures 14 and 15 show the results of this analysis for January and July, respectfully. This figures show the historical and modeled data for in January and July 1974 to 2015. The figure shows the historical data, and the mean, mean plus one standard deviation, and mean minus one standard deviation of the modeled data. In addition, a linear trend-line associated with each of these data sets is provided in the figures.

13
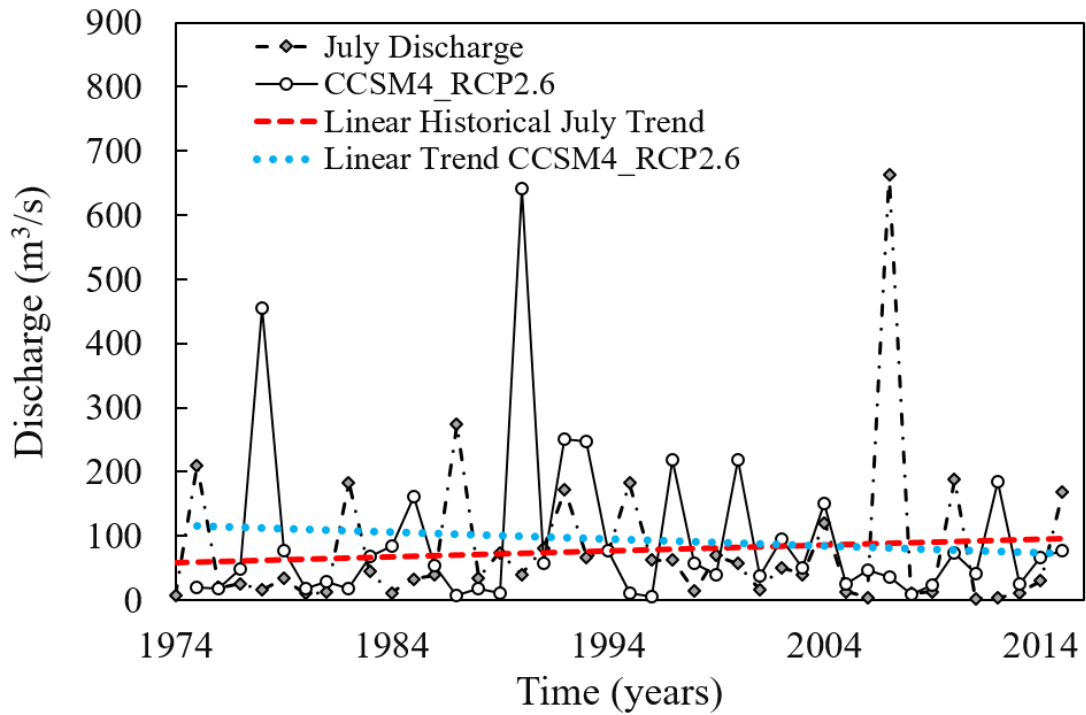
Figure 13. Historic river discharge data compared to CCSM4_RCP2.6 model data for the month of July 1974 to 2015
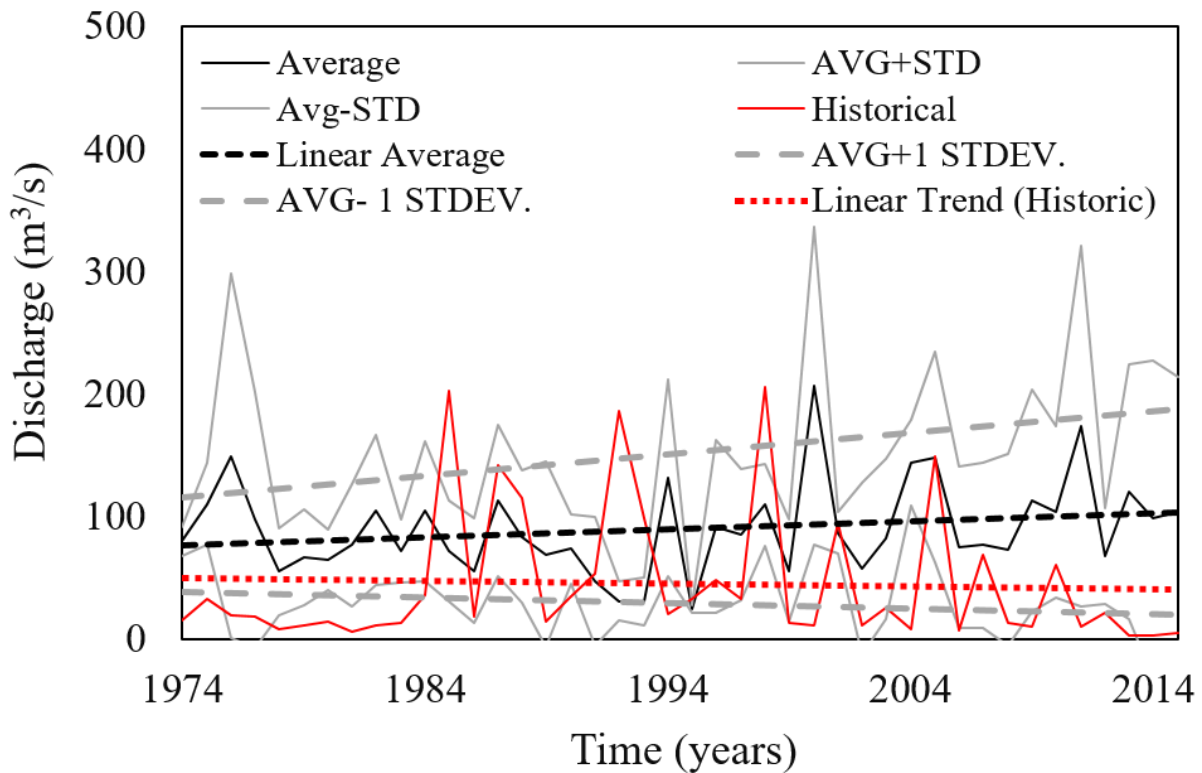
Figure 14. Model average versus historic data for January 1974-2015
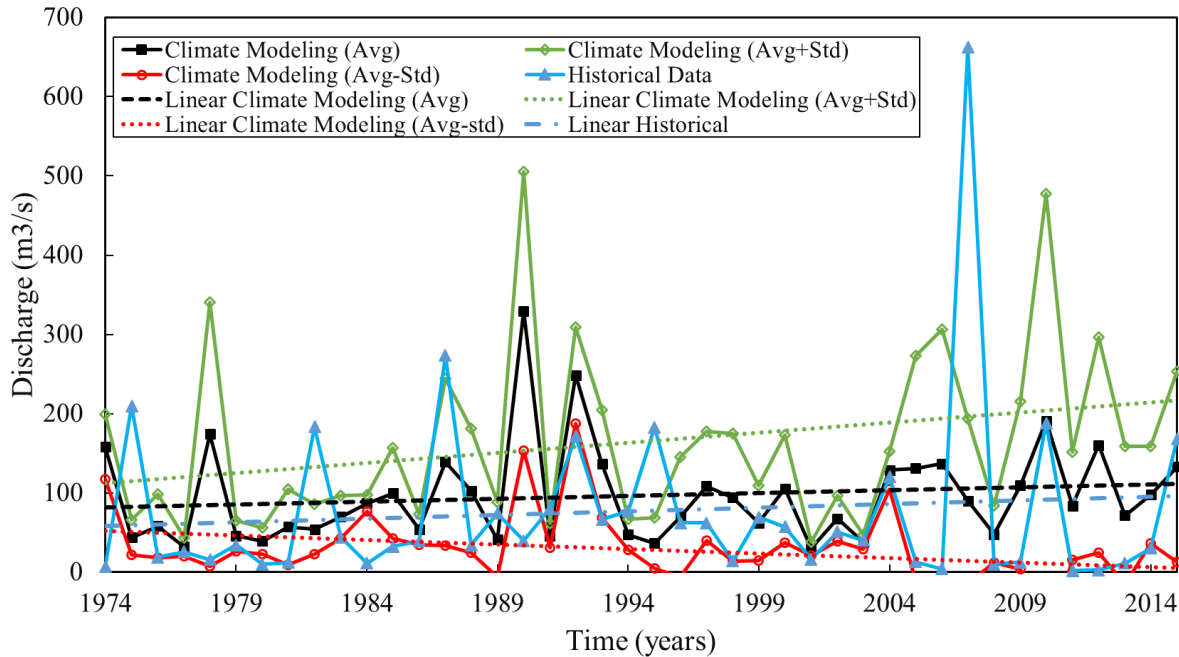
Figure 15. Model average versus historical data for July 1974-2015

From January data presented in Figure 14, it is observed that the average trend lines for the model and the historical data do not coincide; however, the model captures the historical data within one standard deviation from the average. Figure 15 presents the same analysis with the July data. With the ability to achieve relatively accurate prediction of historic data, the data set was expanded to include future data points associated with all the models, as well as the past records. This comprehensive data set was next used to predict the future risk of bridge failure under flood and flood-induced scour. As before, the BCQM downscaled data is not included in the analysis. The daily discharge of the 18 climate scenarios are averaged and the daily standard deviation was also computed. For the time span January 1, 1961 to December 31, 2099. This data is then plotted against the average daily discharge from January 1974 to January 2015. The results are shown in Figure 16.

15
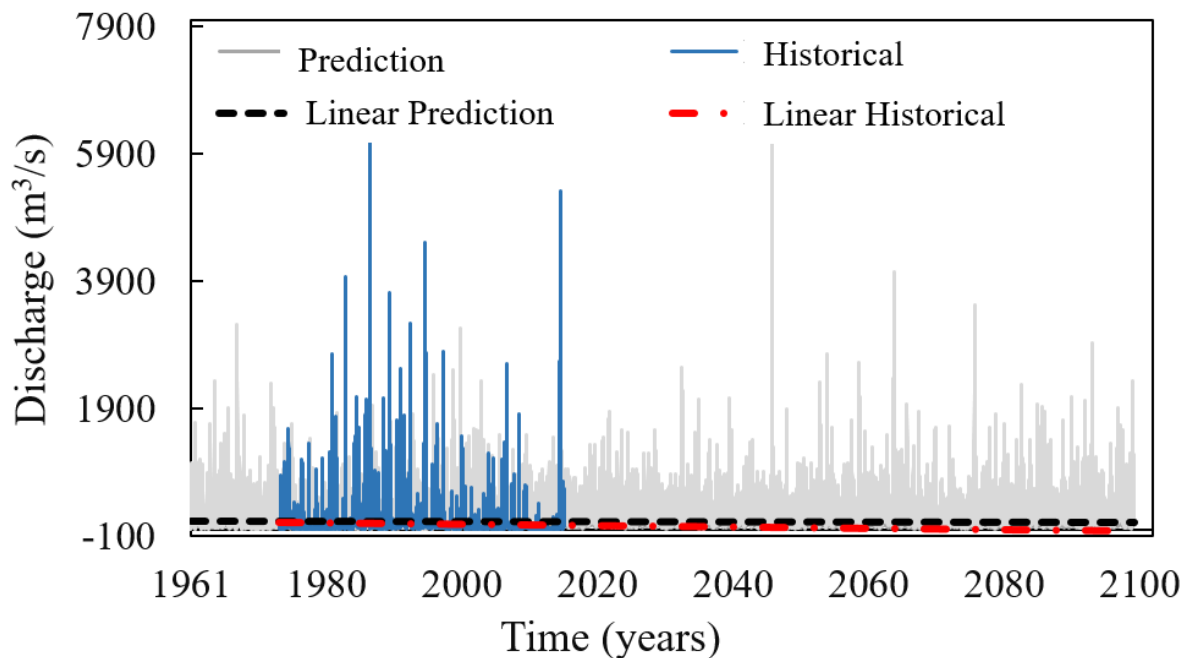
Figure 16. Prediction average versus historical daily streamflow 1961-2099

Figure 16 shows that both the model average and the historical data discharge trends are declining. Based on the results of this plot, the model average tends to be a relatively good predictor for future discharge; however, as with every statistical prediction, the accuracy tends to decrease overtime as suggested by the increasing standard deviations (see Figure 15).

TIME DEPENDENT SCOUR PREDICTION

Flood induced scour significantly affects the time-variant strength and stability of bridges that are subjected to flood conditions. Bed material characteristics, bed configuration, flow characteristics, fluid properties, and the geometry of the pier and footing are recognized as factors that govern the local scour at piers. In the U.S. bridge design and assessment practice, design specifications such as the AASHTO LRFD (2010) include recommendations for design of bridge piers against scour, which requires this design to be performed on the basis of an approved method for scour predictions. These methods are generally based on equations that provide the maximum expected scour depth. The foundations must be placed under this depth to avoid scour failure. In this project, the

scour depth at piers is calculated as HEC-18 (kon et al. 1993) which was established using a set of flume tests considering different soil conditions. HEC-18 provisions for calculating maximum scour depth is defined as follows:

$$d_s = 2k_1 k_2 k_3 \left(\frac{b}{y_0}\right)^{0.65} F_0^{0.43} \tag{1}$$

$$F_0 = \frac{V}{(gy_0)^{0.5}} \tag{2}$$

In which d_s is scour depth, k_1 is correction factor for pier nose shape, k_2 is correction factor for angle of attack of flow, k_3 is correction factor for bed condition, b is pier width, y_0 is flow depth at upstream of the pier, V is velocity of flow in upstream, and F_0 is Froude number. Finally, the time dependent scour depth is calculated using the multi flood accumulation model proposed in Briaud, et al. (1999). This model is suitable for evaluating the time dependent scour depth in cohesive soils where the equilibrium scour may not be reached during a single flood event. In this model, the velocity histogram is assumed to be a step function with a constant velocity value for each step (Kwak, 2001). In case of quantifying the time dependent scour depth, two general cases may happen, case one is when a small flood is followed by a big flood and case two is when a big flood is followed by a small flood. In case one, the scour depth continues to increase after flood one. While in case two, the scour depth due to flood two cannot initiate any additional scour and the scour depth remains constant. Since, the scour holes are assumed to remain intact between the floods, this model represents the worst case scenario that might happen due to the floods. Figure 17 shows the multi-flood accumulation methodology adopted in both cases.
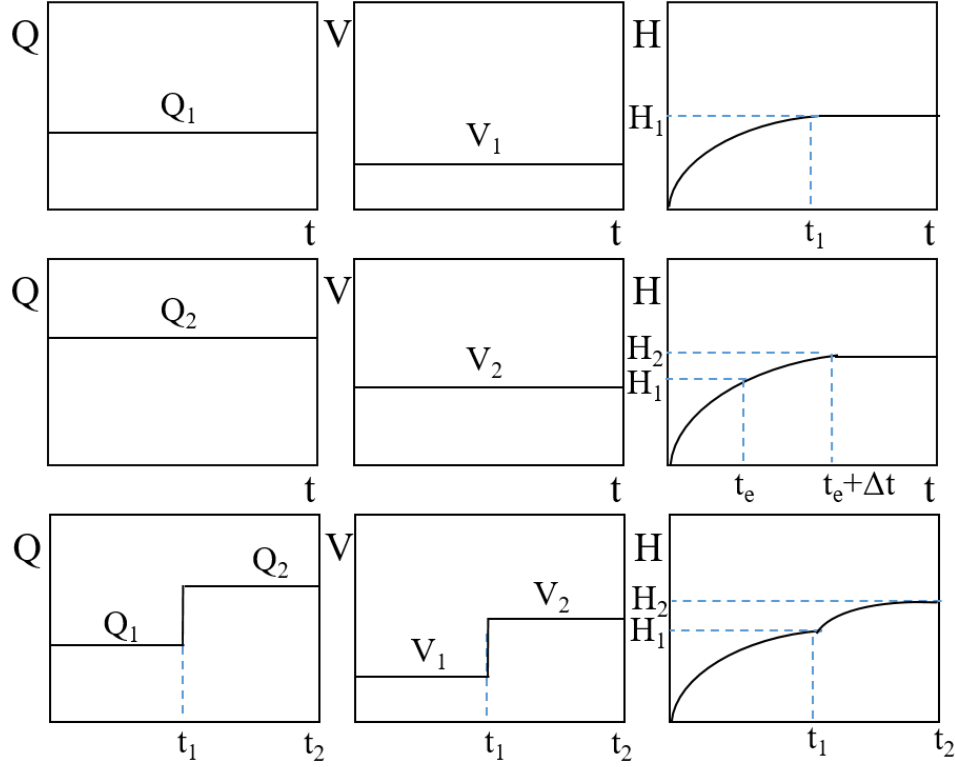
Figure 17. Schematic flood accumulation methodology (adapted from Briaud et al. 1999)

CAPACITY OF BRIDGE FOUNDATIONS

Although the proposed risk assessment approach is similarly applicable to various types of bridge foundation, this project focuses on the capacity of bridges constructed using pile foundations. Lateral and axial failure limit states are defined to assess the behavior of this foundation type under horizontal and vertical loads and compute the failure probability. The ultimate lateral load carrying capacity H_L of one pile is (Prasad and Chari 1999)

$$H_L = 0.3\left(\eta K_P^2 + \xi K \tan \delta\right) \gamma a B (2.7a - 1.7L) \tag{3}$$

with

$$a = \frac{-\left(0.567L + 2.7e\right) + \left(5.307L^2 + 7.29e^2 + 10.541eL\right)^{0.5}}{2.1996} \tag{4}$$

where η is shape factor to account for the non-uniform distribution of earth pressure, K_p is passive earth pressure coefficient, K is lateral earth pressure coefficient, δ is interface

friction angle between the pile and the soil, γ is effective unit weight of soil, a is depth to the point of rotation, B is diameter or width of the pile, L is embedded length of pile, and e is eccentricity of loading. In this model, the shear resistance contribution from both the front soil and side soil is taken into account. In order to evaluate the capacity of each pile in the pile group, a reduction factor is applied to the capacity of a single pile (Hannigan et al. 1997). An equivalent circular diameter of H-pile is computed based on Reese and Van Impe (2010).

The ultimate axial load carrying capacity R_v is expressed as a sum of shaft resistance and toe resistance of a pile as:

$$R_V = R_s + R_p \tag{5}$$

$$R_s = f_s A_s \tag{6}$$

$$R_p = q_p A_p \tag{7}$$

where, R_s is the shaft resistance and R_p is the toe resistance of the piles. f_s is unit shaft resistance over the pile surface area, A_s is pile shaft surface area, q_p is unit toe resistance over the pile toe area, and A_p is pile toe area.

BRIDGE RISK ANALYSIS

The proposed risk assessment approach contains four main modules, namely climate modeling, load prediction, resistance analysis, and probabilistic structural performance evaluation. First, the downscaled climate data are extracted from the appropriate GCMs and streamflow time-histories are generated. The live, dead, and flood induced loads are estimated based on bridge dimensions and discharge data. Scour effects are then quantified and the lateral and axial resistance of bridge foundations are quantified. Finally, the time dependent failure probability and risk profiles are established based on defined axial and lateral failure limit states. This process is performed using probabilistic analysis and Monte Carlo simulation. A layout of the risk analysis framework proposed in this report is shown in Figure 18.
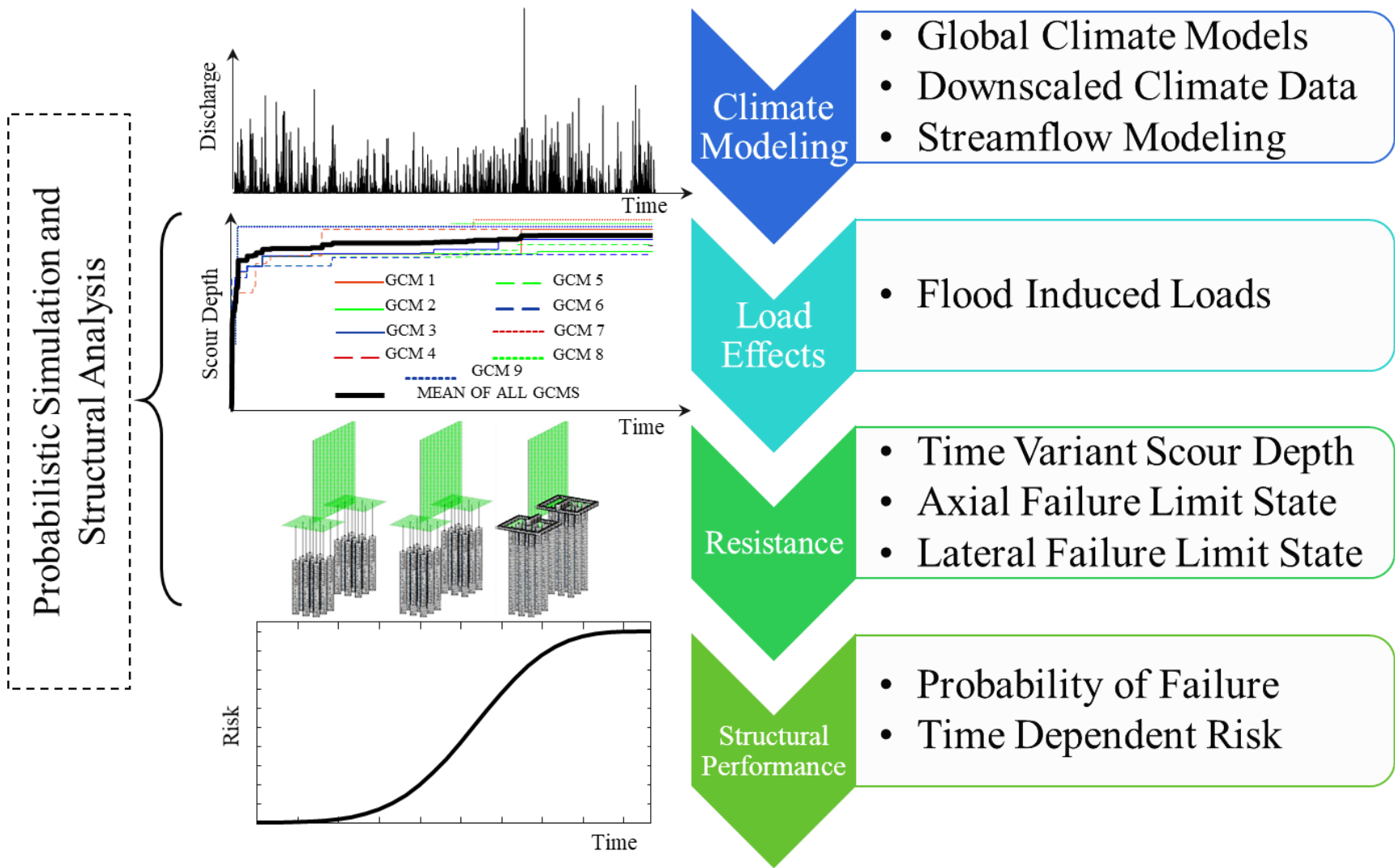
Figure 18. Layout of the proposed risk analysis approach

The proposed framework of this study contains four main modules: (a) climate data analysis and river flow prediction, (b) estimating load effects, (c) resistance evaluation, and (d) predicting time-dependent performance profile. As the first step of this framework, suitable global climate models for the region of interest should be selected. Next, the downscaled precipitation and temperature profiles are analyzed and the river streamflow is predicted. In this study, a hybrid conceptual-metric tool is employed in the streamflow modeling. The resulting streamflow prediction profiles are then used to predict scour depth and assess the structural performance. Next, the probability of bridge failure is found using probabilistic simulations. The last step of this framework is focused on estimating the consequences of bridge failure and establishing the time-dependent risk profile.

In this approach, bridge piers are subjected to traffic live loads and dead loads computed using the AASHTO LRFD Bridge Design Specifications (AASHTO 2014). In addition, flood-induced lateral load FL acting on bridge pier is calculated as (Cuomo et al. 2008):

$$F_L = p \times A \tag{8}$$

With

$$p = C_D \frac{\gamma}{2g} V_{appr}^2 \tag{9}$$

where A is the area of accumulated debris, p is water pressure on piers, C_D is drag coefficient, and V_{appr} is velocity of stream flow.

For deep pile foundations, failure will happen when axial or lateral forces exceed the foundation capacity reduced due to scour formation. In such case, the lateral and axial failure limit states can be defined based on pile capacity models discussed above. These performance functions are defined as

$$G_v(t) = R_v(t) - L_v(t) \tag{10}$$

$$G_l(t) = R_l(t) - L_l(t) \tag{11}$$

where $G_l(t)$ and $G_v(t)$ are lateral and vertical performance functions at time t, respectively, $R_v(t)$ and $R_l(t)$ represent the respective time-variant vertical and lateral capacities, and

$L_v(t)$ and L_l (t) are the respective vertical and lateral load effects at time t. These performance functions are used to evaluate the probability of failure and risk due to flood and flood-induced scour. The point-in-time probability of failure is

$$P_f(t) = P [any\ G_i(t) < 0] \tag{12}$$

where $P_f(t)$ is point-in-time probability of failure and $G_i(t)$ is the ith performance function. The probability of failure us computed using Monte Carlo simulation executed in MATLAB environment with 100,000 random samples to properly consider various uncertainties. The system failure probability is computed as the failure probability with failure modes connected in series. The cumulative annual probability of failure $TDP(y_t)$, representing the cumulative distribution function of the time to failure, is computed as (Decò and Frangopol 2011)

$$TDP(y_t) = \sum_{i=1}^{t} \left(P_{f,i} \prod_{j=1}^{i} (1 - P_{f,j-1}) \right) \tag{13}$$

Finally, the risk of structural failure is calculated based on the evaluated failure consequences as

$$Risk\ (t) = TDP\ (y_t) \times C \tag{14}$$

where $Risk\ (t)$ is the time dependent risk, and C represents the direct and indirect consequences of failure calculated based on rebuilding cost, running cost, and time loss due to the bridge failure and/or road closure due to maintenance and repairs. Equation 6 shows the relationship between these terms (Stein et al. 1999).

$$C = C_{R1} + C_{R2} + C_{R3} \tag{15}$$

in which the rebuilding cost (C_{R1}) is estimated as a function of bridge area considering length and width of the bridge. This cost is computed as

$$C_{R1} = C_{rc} \times W_b \times L_b \tag{16}$$

where C_{R1} is total rebuilding cost (\$), C_{rc} is rebuilding cost (\$) per unit area, W_b is bridge width (m), and L_b is bridge length (m). The running cost represents the additional required cost of vehicles on detour due to bridge closure and it is calculated as

$$C_{R2} = C_{rv} \times D \times ADT \times d \tag{17}$$

where C_{R2} is total running cost (\$), C_{rv} is average cost of running vehicle (\$/km), D is detour length (km), ADT is average daily traffic affected by bridge closure (vehicles/day), and d is duration of detour (days). The time loss cost as a function of additional time loss for passenger cars and trucks is calculated as

$$C_{R3} = \left[C_1 O \left(1 - \frac{T}{100} \right) + C_2 \frac{T}{100} \right] \frac{DAd}{S} \qquad (18)$$

with C_{R3} representing the total cost of time loss (\$), C_1 is value of time per adult (\$/hr.), C_2 is value of time for truck (\$/hr.), S is average detour speed (km/hr.), T is average daily truck traffic (%), and O is occupancy rate.

CASE STUDY

The presented framework is illustrated on the South Bound I-35 Bridge over the Red River. The bridge serving a major freight route linking Southern and Northern US states is located on the Oklahoma-Texas border. This bridge accommodates an average daily traffic of 19,800 vehicles with 36% average daily truck traffic (FHWA 2016). During the past few decades, the Red River has experienced several heavy floods which caused significant damage to surrounding areas. The most recent severe flood occurred in May 2015, in which the water reached the level of the superstructure. In addition, several other bridges along the Red River basin experienced partial or total failure during this flood season (Fechter 2015; Danner and Fuller 2015). The I-35 bridge represents an ideal example due to its strategic location on a major freight route, the aggressiveness of flooding conditions on the Red River, the large daily traffic utilizing the bridge, and the lack of alternative routes in case of bridge failure. Figure 19 shows the location of the bridge on the I-35 over the Red River.

The I-35 bridge superstructure consists of five steel plate girders supporting a reinforced concrete deck, while the substructure is composed of multiple piers supported by steel H-piles. The bridge is 118.3 *m* long and 9.5 *m* wide, with two traffic lanes. The bridge has 11 piers and 32.3 *m* long spans. Since not all the characteristics of the bridge could be obtained, some assumptions related to dimensions were placed. These include the

thickness of the concrete deck (35 *cm*) and the width of the bridge piers (1.2 *m*). Based on the original construction drawings, the riverbed level is considered to be 10 *m* below the deck. In this study, the failure risk analysis has been performed considering a single pier. However, system analysis covering all the piers can be performed using series-system reliability formulation. The studied bridge pier has two groups of 9 steel H-piles (HP 12x53 steel piles), each is 11.2 *m* long. Piles are aligned such that their strong axis is perpendicular to the direction of streamflow.

CLIMATE MODELING, FLOOD, AND SCOUR PREDICTION

The streamflow data using MPI_ESM_LR, CCSM4, and MIROC5 global climate models downscaled with BCQM and CDFt methods and RCP 2.6, RCP 4.5, and RCP 8.5 for the location of interest are adopted from McPherson (2016). The combination of three GCMs, three RCP values, and two downscaling methods results in eighteen different streamflow datasets. These datasets are implemented in the proposed risk assessment approach to quantify the risk of I-35 bridge failure.

Figure 19. Geographical location of the I-35 bridge over Red River (Google 2018)

Scour modeling for each streamflow time-series, corresponding to a given climate scenario, is performed using the Equation (1). The results of maximum scour depth prediction are obtained using the method proposed in Briaud, et al. (1999). The time-

dependent scour depth associated with different climate scenarios is then established. Figure 20 shows the time dependent scour depth profiles for all climate scenarios. As shown, there is a considerable variability in the scour depths among the considered scenarios. The results depict up to 45% difference in final scour depth between different climate datasets. This highlights the significant uncertainty associated with the scour prediction considering climate change and justifies the need for probabilistic analysis.
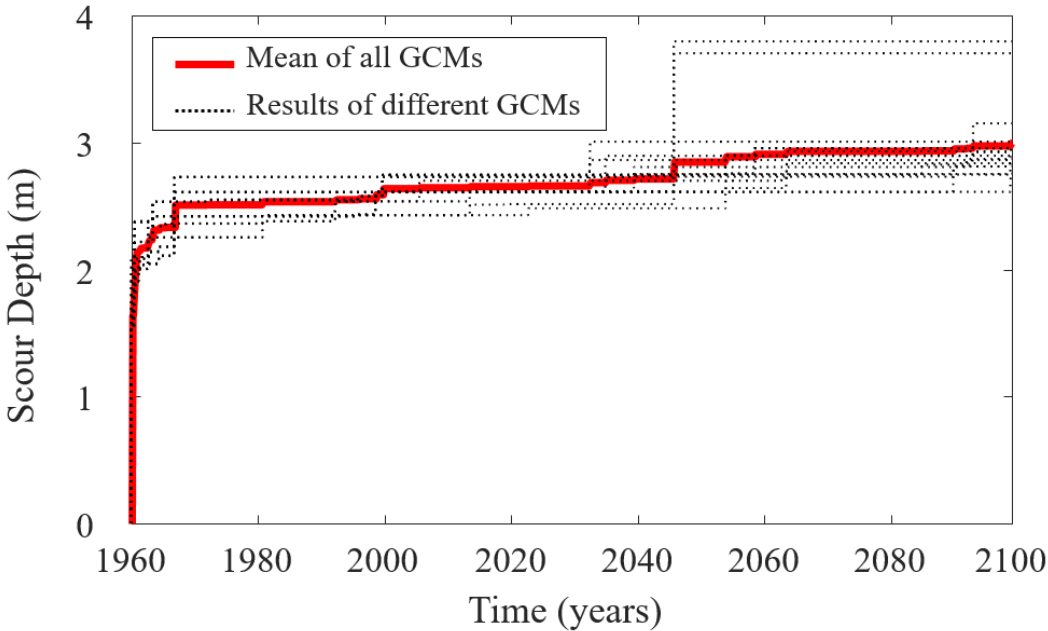
Figure 20. Time dependent scour depth results based on different GCMs

TIME DEPENDENT RISK ASSESSMENT

In order to consider the uncertainties associated with load and resistance effects in performance prediction, Monte Carlo simulation with 100,000 samples is used to draw samples from the time-variant scour depth at the investigated bridge pier. Next, each sample from the distribution is used to perform the time dependent scour depth prediction. The internal friction angle of soil is considered as a random variable that follows a normal distribution with mean value of 36° and standard deviation of 1.33 (Fellenius 1991). The unit weight of saturated soil is assumed 124 lbs /ft³, and coefficient of lateral earth pressure is assumed 0.4. In addition to soil parameters, the streamflow is treated as a

random variable. The predicted streamflow of each year is used to predict the parameter of the best exponential distribution fit and Monte Carlo simulation is used to find the annual histograms of the time-variant scour depth. The probabilistic scour depth is next used to calculate probability of failure using the performance functions given by Equations (10) and (11). Axial and vertical load capacity of the piles are calculated using equations (3) and (5). Figure 21 shows the probabilistic time-variant capacity of the piles in lateral and axial directions. Vertical loads from traffic and dead load of the structure are calculated based on AASHTO LRFD Specifications (AASHTO 2014) considering HL-93 loading to obtain maximum vertical forces on the bridge supports. Lateral load due to discharge is calculated using Equation (8). With the probabilistic load and capacity terms in the limit state functions identified, the annual probability of failure can be obtained using the Monte Carlo simulation results.

After establishing the failure probability profiles, consequences due to bridge failure are evaluated considering repair cost, running cost, and time loss cost, calculated using Equations (16), (17), and (18), respectively. The failure risk is then computed using Equation (14). All the parameters used in calculating the consequences are considered random variables, except the detour length (D) and the duration of detour (d). Table 1 presents the values of deterministic parameters and the descriptors of randomly distributed parameters used in calculating the failure risk.

In this study, it is assumed that the effect of inflation negates the money interest; accordingly, the discount rate of money is assumed to be zero. The detour length is derived by analysis of the transportation network to which the bridge belongs. The area on the I-35 before and after the bridge is analyzed to identify alternative routes in case of bridge failure. The analysis indicates that the average travel time is 25 minutes with the intact bridge, while the detour will result in an average of 60 minutes travel time in case of bridge failure. In order to compute the failure probability and risk, Monte Carlo simulation with 100,000 samples is adopted. Figure 22 shows the mean, mean plus one standard deviation, and mean minus one standard deviation of time dependent risk profile.
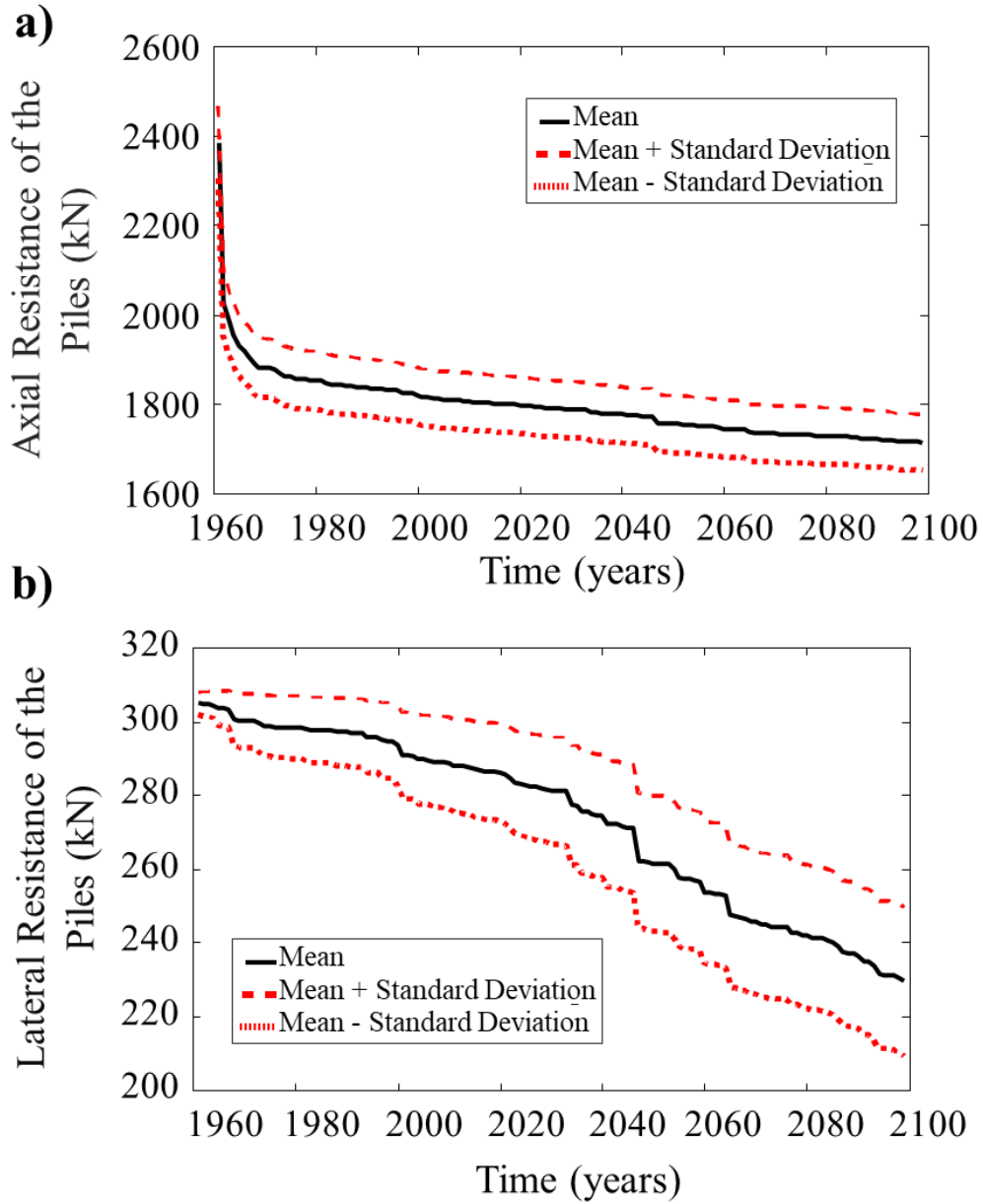
Figure 21. Time variant resistance of piles in (a) axial (b) lateral directions

Table 1. Parameters for evaluation of rebuilding, running, and time-loss costs

| Parameter	Notation	Value	Probabilistic Parameters	References
Rebuilding cost ($/m²)	Crc	$894 / m²	Lognormal, COV= 0.2	Deco & Frangopol (2011)
Average cost of running vehicle ($/km)	Crv	$0.08 / km	Lognormal, COV = 0.2	Deco & Frangopol (2011)
Detour Length	D	90 km	Deterministic	Estimated based on analysis of traffic network
Average Daily Traffic	ADT	19,800 vehicles/day	Lognormal, COV = 0.2	FHWA (2016)
Duration of detour	d	182.5 days (6 months)	Deterministic	Assumed
Cost of time per adult ($/hr.)	C_1	$22.82	Lognormal, COV = 0.15	Deco & Frangopol (2011)
Cost of time for truck ($/hr.)	C_2	$26.97	Lognormal, COV = 0.15	Deco & Frangopol (2011)
Average detour speed (km/hr.)	S	64	Lognormal, COV = 0.15	Deco & Frangopol (2011)
Average daily truck traffic	T	36%	Lognormal, COV = 0.2	FHWA (2016)
Occupancy rate	O	1.5 adults	Lognormal, COV = 0.15	Deco & Frangopol (2011)
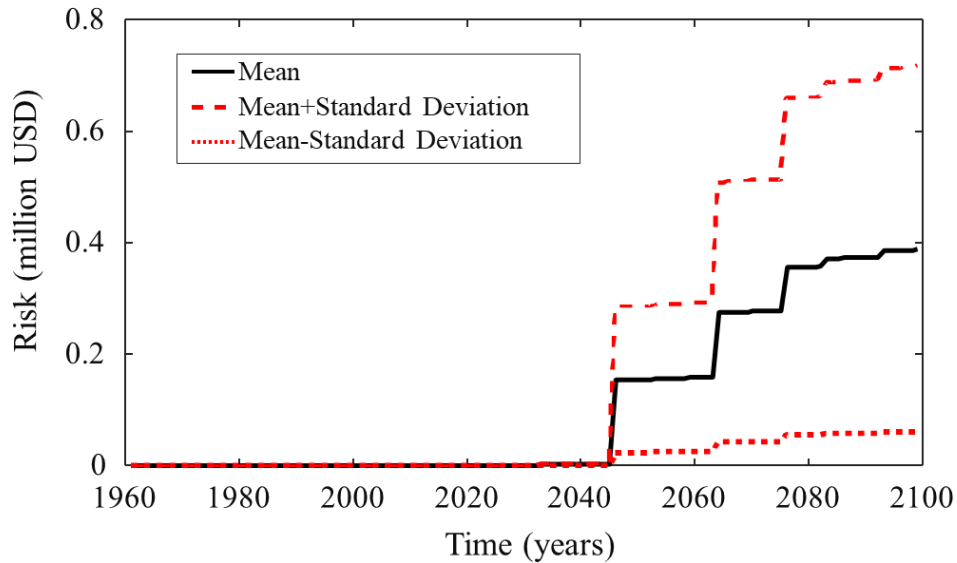
Figure 22. The mean value of time dependent risk based on all climate models

EFFECT OF CLIMATE CHANGE ON GRADUAL DETERIORATION OF BRIDGES

In addition to the impacts on flood hazard occurrence and scour progression, climate change could also affect the corrosion propagation rate in structural components due to the change in carbon dioxide concentration, temperature, and humidity at a given location. These changes may occur due to carbonation or chloride penetration to steel reinforcement. Specifically, the increase in temperature profiles increases the material diffusivity and consequently increases the corrosion rate in reinforcement (Stewart, et al. 2012).

In addition, in case of steel structures and in particular steel piles which play vital role in the maintaining the stability of large number of bridges and marine structures, Chaves et al. (2016) conducted probabilistic analysis on corrosion of steel marine structures under global warming and nutrient pollution. Their proposed methodology, applied to marine piles, highlights the significant role of seawater temperature and microbiological nutrients on corrosion estimation. Results of their study indicated that the long-term reliability of the structure is highly likely to be affected by the increase of marine nutrients; the marine nutrients may also increase due to global warming.

Stewart et al. (2011 and 2012) and Wang et al. (2012) considered the effects of climate change on the corrosion initiation and propagation in reinforced concrete structures. In most of these studies, temperature and carbon dioxide emission scenarios based on the global climate models are implemented in the structural deterioration prediction process.

Additionally, probabilistic analysis which considers the effect of uncertainties associated with CO_2 concentration, material properties, dimensions, and modeling procedure is presented. The results of these studies indicates a growing risk due to carbonation- and chloride-induced corrosion. Although, significant research in quantifying the effect of climate change on risk of corrosion initiation and progression has been conducted, the current review of the literature shows that such quantification has yet to find its way to maintenance and repair optimization procedures implemented in bridge management approaches.

LIFE-CYCLE MANAGEMENT AND RISK-BASED MAINTENANCE OPTIMIZATION

Infrastructure decision making process is generally affected by the strict budgetary constraints and limited resources available for maintenance and repair operations. Therefore, using optimization techniques could result in achieving an appropriate and efficient life-cycle management solutions. These techniques are capable of providing a balance between conflicting life-cycle management criteria (e.g., total maintenance cost and expected service life). Optimization techniques can provide the optimal management activities as the solution of an optimization problem that simultaneously minimizes the life cycle costs and maximizes expected life-cycle management cost.

An efficient framework for life cycle management should consist of modules for performance prediction under single or multiple hazards, intervention optimization, reliability and cost-informed decision making. Examples of this type of management frameworks can be found in Frangopol and Soliman (2016). Figure 23 shows a schematic view of such frameworks. Several modules are used in this framework. The first module identifies the deterioration mechanisms and hazards that would affect the structural performance. Next, the consequences of failure are estimated and the performance of

structure is evaluated. The results of inspection and structural health monitoring are also integrated in this framework. Improved structural performance predictions are then employed and the optimum maintenance and management strategies are established to assist in decision making regarding future bridge interventions.
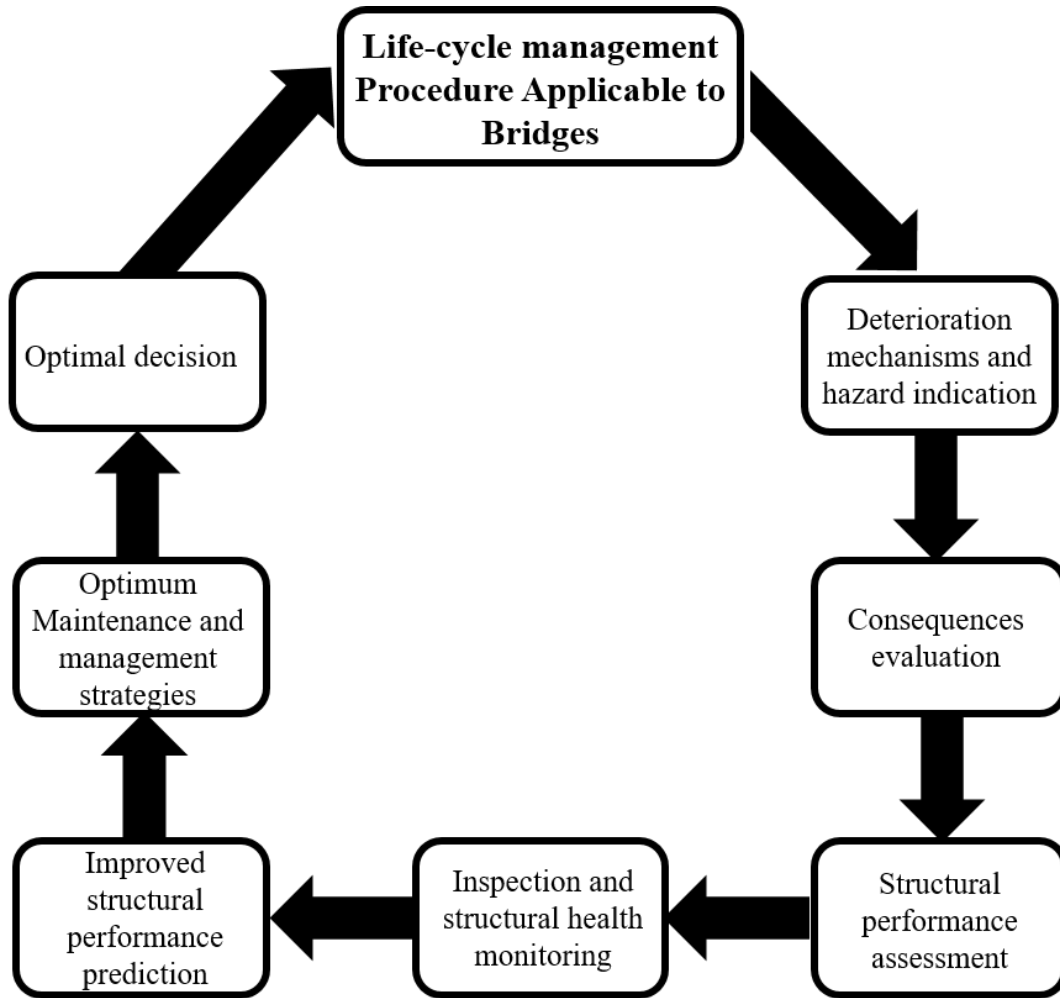
Figure 23. General life-cycle management procedure for bridges

In general, multi-objective optimization procedures would provide several solutions to the optimization problem. The decision-makers can choose their best alternatives based on the problem constrains or any other practical considerations. However, several methods can also be used to assist in the decision-making process. For instance, the relative desirability of maintenance strategies can be investigated using utility theory. This theory provides a utility value for each management alternative based on the decision-maker's preferences and attitude. The relative values can then be measured, combined, and

compared using to establish the best solution based on the decision-maker's preferences (Ang and Tang, 1984). The decision-making process based on this approach has been integrated into bridge management in Sabatino et al. (2015).

CONCLUSIONS

This report presented a probabilistic framework for risk assessment of bridges under flood and flood-induced scour considering climate change. The flood and streamflow prediction is performed using Global Climate Models which result in streamflow time-histories for the time span of 1961 to 2100 at the investigated bridge location. Time-dependent scour depth is quantified and its effect on the axial and lateral capacity of the bridge foundation is computed. The annual point-in-time failure probability of the bridge due to flood-induced loads is used to predict the cumulative failure probability profiles of the bridge. After evaluating the consequences associated with bridge failure, the time-variant bridge risk profile is established. In addition, a risk-based probabilistic framework for optimizing the management activities of bridges susceptible to damage due to floods, flood-induced scour, and corrosive environment is discussed. The following conclusions are drawn:

- The time-variant scour depth significantly depends on the adopted climate scenarios. A variation of 45% in the final scour depth predicted using different climate scenarios has been observed at the studied location. Accordingly, a probabilistic approach considering potential scenarios is necessary to properly quantify the risk of bridge failure due to flood and flood-induced scour hazards.

- The data analysis for the investigated location has shown that precipitation events have become increasingly variable and indications of wetting months shifting further from normal has been observed.

- For the investigated location, the RCP 2.6 associated with each model predicts the highest scour depth, while the 8.5 RCP values predict the lowest scour depth profiles.

- The proposed approach based on climate models provides a rational prediction of future risk while properly accounting for uncertainties associated with future climate and flood conditions.

32

- The proposed risk quantification approach can be integrated into an optimization framework to establish the optimum maintenance solutions which minimize the total life-cycle cost of the bridge under investigation and maximizes its service life.

REFRENCES

AASHTO. (2010). American association of state highway and transportation officials (LRFD) bridge design specifications. 5th Ed., *Washington, DC.*

AASHTO. (2014). American association of state highway and transportation officials (LRFD) bridge design specifications. 6th Ed., *Washington, DC.*

Ang, A. H., and Tang, W. H. (1984). Probability concepts in engineering planning and design, Volume II. Decision, risk, and reliability. *John Wiley and Sons, Inc.,* New York, NY.

Arneson, L.A., Zevenbergen, L.W., Lagasse, P.F., & Clopper, P.E. (2012). Evaluating scour at bridges. *Hydraulic Engineering Circular No. 18: FHWA-HIF-12-003*, U.S. DOT, Washington, DC.

Bolduc, L., Gardoni, P., & Briaud, J.-L. (2008). Probability of exceedance estimates for scour depth around bridge piers, *Journal of Geotechnical and Geoenvironmental Engineering, 134*(2), 175–184.

Briaud, J. L., Gardoni, P., & Yao, C. (2013). Statistical, risk, and reliability analyses of bridge scour. *Journal of Geotechnical and Geoenvironmental Engineering, 140*(2), 04013011.

Briaud, J. L., Ting, F. C., Chen, H. C., Gudavalli, R., Perugu, S., & Wei, G. (1999). SRICOS: Prediction of scour rate in cohesive soils at bridge piers. *Journal of Geotechnical and Geoenvironmental Engineering, 125*(4), 237-246.

Briaud, J.-L., Brandimarte, L., Wang, J., & D'Odorico, P. (2007). Probability of scour depth exceedance owing to hydrologic uncertainty. *Georisk: Assessment and Management of Risk for Engineered Systems and Geohazards, 1*(2), 77-88.

Chaves, I. A., Melchers, R. E., Peng, L., and Stewart, M. G. (2016). Probabilistic remaining life estimation for deteriorating steel marine infrastructure under global warming and nutrient pollution. *Ocean Engineering, 126,* 129-137.

Coiffier, J. (2011). *Fundamentals of numerical weather prediction.* Cambridge University Press.

Cook, W., Barr, P.J., & Halling, M.W. (2015). Bridge failure rate. *Journal of Performance of Constructed Facilities, 29*(3), 04014080.

Croke, B. F. W., Andrews, F., Spate, J., & Cuddy, S. M. (2005). *IHACRES user guide.* Technical Report 2005/19. Second Edition. iCAM, School of Resources, Environment and Society, The Australian National University, Canberra.

Cuomo, G., Shams, G., Jonkman, S., & Van Gelder, P. (2008). Hydrodynamic loadings of buildings in floods. *Coastal Engineering*, 3745.

Danner, C., & Fuller, J., (2015). Texas and Oklahoma begin cleaning up after devastating floods. Retrieved from: http://nymag.com/daily/intelligencer/2015/05/floods-devastate-texas-and-oklahoma.html

Decò, A., & Frangopol, D. M. (2011). Risk assessment of highway bridges under multiple hazards. *Journal of Risk Research*, *14*(9), 1057-1089.

Ettouney, M. M., & Alampalli, S. (2011). Infrastructure Health in Civil Engineering: Applications and Management. *CRC Press*, Taylor and Francis Boca Raton, Florida.

Fechter, J. (2015). TXDoT: Two bridges completely wrecked in Central Texas floods, others damaged. Retrieved from: http://www.mysanantonio.com/news/local/article/TXDoT-Two-bridges-wrecked-in-the-Central-Texas-6294892.php#photo-8045574

Fellenius B.H. (1991) *Pile Foundations*. In: Fang BY. (eds) Foundation Engineering Handbook. Springer, Boston, MA.

FHWA (Federal Highway Administration). (2016). National bridge inventory (NBI) dataset. Retrieved from: https://www.fhwa.dot.gov/bridge/nbi/ascii2016.cfm

Frangopol, D. M., and Soliman, M. (2016). Life-cycle of structural systems: recent achievements and future directions. *Structure and infrastructure engineering*, *12*(1), 1-20.

Gehl, P., & D'Ayala, D. (2016). Development of Bayesian networks for the multi-hazard fragility assessment of bridge systems. *Structural Safety, 60*, 37-46.

Gent, P. R., Danabasoglu, G., Donner, L. J., Holland, M. M., Hunke, E. C., Jayne, S. R., ... & Worley, P. H. (2011). The community climate system model version 4. *Journal of Climate*, *24*(19), 4973-4991.

Giorgetta, M. A., Jungclaus, J., Reick, C. H., Legutke, S., Bader, J., Böttinger, M., ... & Glushak, K. (2013). Climate and carbon cycle changes from 1850 to 2100 in MPI-ESM simulations for the Coupled Model Intercomparison Project phase 5. *Journal of Advances in Modeling Earth Systems*, *5*(3), 572-597.

Google Maps. (2018). *I-35 Red River Bridge*. Retrieved from https://goo.gl/maps/pAro4JLDw542

Govindasamy, A.V., Briaud, J., Chen, H., Delphia, J., Elsbury, K., Gardoni, P., Herrman, G., Kim, D., Mathewson, C., McClelland, M., & Olivera, F. (2008). Simplified method for estimating scour at bridges, *GeoCongress 2008, Geosustainability and Geohazard Mitigation, 178*, 385-393.

Hannigan, P. J., Goble, G. G., Thendean, G., Likins, G. E., & Rausche, F. (1997). *Design and construction of driven pile foundations-Volume ii* (No. FHWA-HI-97-014).

Ho, C. K., Stephenson, D. B., Collins, M., Ferro, C. A., & Brown, S. J. (2012). Calibration strategies: a source of additional uncertainty in climate change projections. *Bulletin of the American Meteorological Society*, *93*(1), 21-26.

Kwak, K. (2001). Prediction of scour depth versus time for bridge piers in cohesive soils in the case of multi-flood and multi-layer soil systems. *KSCE Journal of Civil Engineering, 5*(1), 67-74.

Laprise, R. (2008). Regional climate modelling. *Journal of Computational Physics, 227*(7), 3641-3666.

Li, H., Sheffield, J., & Wood, E. F. (2010). Bias correction of monthly precipitation and temperature fields from Intergovernmental Panel on Climate Change AR4 models using equidistant quantile matching. *Journal of Geophysical Research: Atmospheres*, *115*(D10).

Liang, X., Lettenmaier, D. P., Wood, E. F., & Burges, S. J. (1994). A simple hydrologically based model of land surface water and energy fluxes for general circulation models. *Journal of Geophysical Research: Atmospheres*, *99*(D7), 14415-14428.

Maloney, E. D., Camargo, S. J., Chang, E., Colle, B., Fu, R., Geil, K. L., Hu, Q., Jiang, X., Johnson, N. & Karnauskas, K. B. (2014). North American climate in cmip5 experiments: part iii: assessment of twenty-first-century projections. *Journal of Climate, 27*(6), 2230-2270.

Maurer, E. P., & Hidalgo, H. G. (2008). Utility of daily vs. monthly large-scale climate data: an intercomparison of two statistical downscaling methods. *Hydrology and Earth System Science, 12*, 551-563.

Maurer, E. P., Hidalgo, H. G., Das, T., Dettinger, M. D., & Cayan, D. R. (2010). The utility of daily large-scale climate data in the assessment of climate change impacts on daily streamflow in California. *Hydrology and Earth System Science, 14*, 1125-1138.

McPherson, R., (2016). SCCSC, South Central Climate Science Center. *Impacts of Climate change on Flows in the Red River Basin*, Final Report, Feb. 2016.

Melillo, J. M., Richmond, T., and Yohe, G. W., eds. (2014) *Climate Change Impacts in the United States: The Third National Climate Assessment*. U.S. Global Change Research Program.

NASA (2017). National Aeronautics and Space Administration, NASA Jet Propulsion Laboratory **https://climate.nasa.gov/**

NOAA (2015). Nuisance flooding, an increasing problem as coastal sea levels rise, National Oceanic and Atmospheric Administration, http://www.noaanews.noaa.gov/stories2014/20140728_nuisanceflooding.html

NOAA (2017). National Oceanic and Atmospheric Administration, http://www.noaa.gov/

Pierce, D. W., Barnett, T. P., Santer, B. D., & Gleckler, P. J. (2009). Selecting global climate models for regional climate change studies. *Proceedings of the National Academy of Sciences*, *106*(21), 8441-8446.

Prasad, Y. V., & Chari, T. R. (1999). Lateral capacity of model rigid piles in cohesionless soils. *Soils and Foundations*, *39*(2), 21-29.

Reese, L. C., & Van Impe, W. F. (2010). *Single piles and pile groups under lateral loading*. CRC Press.

Richardson, E. V., Harrison, L. J., Richardson, J. R., & Davis, S. R. (1993). *Evaluating scour at bridges* (No. HEC 18 (2nd edition))

Sabatino, S., Frangopol, D. M., and Dong, Y. (2015). Sustainability-informed maintenance optimization of highway bridges considering multi-attribute utility and risk attitude. *Engineering Structures*, *102*, 310-321.

Sachindra, D. A., Huang, F., Barton, A., & Perera, B. J. C. (2014). Statistical downscaling of general circulation model outputs to precipitation—part 2: bias-correction and future projections. *International Journal of Climatology*, *34*(11), 3282-3303.

Seager, R., Ting, M., Held, I., Kushnir, Y., Lu, J., Vecchi, G., ... & Li, C. (2007). Model projections of an imminent transition to a more arid climate in southwestern North America. *Science*, *316*(5828), 1181-1184.

Sheffield, J., Barrett, A. P., Colle, B., Nelun Fernando, D., Fu, R., Geil, K. L., Hu, Q., Kinter, J., Kumar, S. & Langenbrunner, B. (2013a). North American climate in CMIP5 experiments. Part I: evaluation of historical simulations of continental and regional climatology. *Journal of Climate, 26*(23), 9209-9245.

Sheffield, J., Camargo, S. J., Fu, R., Hu, Q., Jiang, X., Johnson, N., Karnauskas, K. B., Kim, S. T., Kinter, J. & Kumar, S. (2013b). North American climate in CMIP5 experiments. Part II: evaluation of historical simulations of intraseasonal to decadal variability. *Journal of Climate, 26*(23), 9247-9290.

Smith, A., Lott, N., Houston, T., Shein, K., Crouch, J., & Enloe, J. (2017). US billion-dollar weather & climate disasters: 1980-2017. *NOAA National Centers for Environmental Information.* https://www.ncdc.noaa.gov/billions/events.pdf.

Solomon, S. (Ed.). (2007). Climate change 2007-the physical science basis: Working group I contribution to the fourth assessment report of the IPCC (Vol. 4). Cambridge University Press.

Stein, S. M., Young, G. K., Trent, R. E., & Pearson, D. R. (1999). Prioritizing scour vulnerable bridges using risk. *Journal of Infrastructure Systems*, *5*(3), 95-101.

Stewart, M. G., Wang, X., and Nguyen, M. N. (2011). Climate change impact and risks of concrete infrastructure deterioration. *Engineering Structures*, *33*(4), 1326-1337.

Stewart, M. G., Wang, X., and Nguyen, M. N. (2012). Climate change adaptation for corrosion control of concrete infrastructure. *Structural Safety*, *35*, 29-39.

Taylor, K. E., Stouffer, R. J., & Meehl, G. A. (2012). An overview of CMIP5 and the experiment design. *Bulletin of the American Meteorological Society*, *93*(4), 485-498.

USGS (2017). United State Geological Survey, National Water Information Service, https://waterdata.usgs.gov/nwis

Vrac, M., & Michelangeli, P. A. (2009). CDFt R Package.

Wang, X., Stewart, M. G., and Nguyen, M. (2012). Impact of climate change on corrosion and damage to concrete infrastructure in Australia. *Climatic change*, *110*(3-4), 941-957.

Wang, Z., Padgett, J.E., & Dueñas-Osorio, L. (2014). Risk-consistent calibration of load factors for the design of reinforced concrete bridges under the combined effects of earthquake and scour hazards. *Engineering Structures*, *79*, 86-95.

Watanabe, M., Suzuki, T., O'ishi, R., Komuro, Y., Watanabe, S., Emori, S., ... & Takata, K. (2010). Improved climate simulation by MIROC5: mean states, variability, and climate sensitivity. *Journal of Climate*, *23*(23), 6312-6335.

Wayne, G. P. (2013). The beginner's guide to representative concentration pathways. *skeptical science*, *25*.

Xue, Y., Janjic, Z., Dudhia, J., Vasic, R., & De Sales, F. (2014). A review on regional dynamical downscaling in intraseasonal to seasonal simulation/prediction and major factors that affect downscaling ability. *Atmospheric research*, *147*, 68-85.

Zagona, E. A., Fulp, T. J., Shane, R., Magee, T., & Goranflo, H. M. (2001). RiverWare: A generalized tool for complex reservoir system modeling. *JAWRA Journal of the American Water Resources Association*, *37*(4), 913-929.